Variability of Net Radiation on Snow-Covered Forest Floor for a Range of Vegetation Densities along a Latitudinal Transect

Bijan Seyednasrollah[1], Mukesh Kumar[1]

[1] Nicholas School of the Environment, Duke University, Durham, NC, USA.

Abstract

Net radiation reaching the forest floor is influenced by vegetation density. Previous studies have confirmed that in mid-latitude conifer forests in Greenville, ME (45.5°N), net radiation decreases and then subsequently increases with increasing vegetation density, for clear sky conditions. This leads to existence of a net radiation minimum at an intermediate vegetation density. With increasing cloud cover, the minimum radiation shifts toward lower densities, sometimes resulting in a monotonically increasing radiation with vegetation density. The net radiation trend, however, is expected to change with location of forests, affecting the magnitude and temporality of individual radiation components. This research explores the variability of net radiation on snow-covered forest floor for different vegetation densities along a latitudinal transect. We especially investigate how the magnitude of minimum/maximum radiation and vegetation density at which they are expressed, changes with site location. To evaluate these, net radiation is calculated using the Forest Radiation Model at six different locations in white spruce (*Picea glauca*) forests across North America, with latitudes ranging from 45 to 66°N. Results show that the variation of net radiation with vegetation density significantly varies between different latitudes. In higher latitude forests, the magnitude of net radiation is generally smaller, and the minimum radiation is exhibited at relatively sparser vegetation densities, for clear sky conditions. For interspersed cloudy sky conditions, net radiation non-monotonically varies with latitude across the sites, depending on the seasonal sky cloudiness and air temperature. Net radiation on north-facing hillslopes is less sensitive to latitudinal location than on south-facing sites.

1 Introduction

Net snowcover radiation on forest floor ($NSRF$) is the primary control on the rate and timing of snowmelt in forested regions [*Aguado*, 1985; *Bohren and Thorud*, 1973; *Elder et al.*, 1991]. Estimation of $NSRF$ depends on accurate evaluation of shortwave radiation, S_{Net}, (direct, diffuse and reflected from snow and canopy) and longwave radiation, L_{Net}, (from tree crown, trunk, sky and snow) components [*Pomeroy et al.*, 2009; *Price*, 1988; *Sicart et al.*, 2006]. Both S_{Net} and L_{Net} radiation components are dependent on vegetation density. With increasing vegetation density, shading fraction on the forest floor increases, and hence S_{Net} decreases. On the other hand as vegetation density increases, the portion of incoming longwave radiation from tree crown and trunk increases, and consequently, L_{Net} increases [*Seyednasrollah et al.*, 2013]. Because of the opposing trends in variation of S_{Net} and L_{Net} with vegetation density, $NSRF$ may exhibit a minimum ($NSRF_{min}$) at moderate vegetation densities in coniferous forests (e.g. in Oregon ~44 ºN [*Reifsnyder and Lull*, 1965] and Maine ~45 ºN [*Seyednasrollah et al.*, 2013]). Similar behavior has been reported based on empirical model results in lodgepole pine forests at ~39 °N latitude [*USACE*, 1956]. The variation of $NSRF$ with vegetation density, however, is influenced by a swath of factors including slope and aspect of the forest floor [*Seyednasrollah et al.*, 2013], climatological characteristics [Lundquist et al., 2013], and tree morphometric characteristics such as tree height and crown's shape, radius, depth and density [*Seyednasrollah and Kumar*, 2013]. For a wide range of vegetation densities, net radiation increases with increasing hillslope angle and the minimum radiation occurs at higher vegetation densities. On the other hand, both $NSRF$ and the density at which radiation is minimum decreases with orientation of hillslope changing from south- to north-facing [*Seyednasrollah et al.*, 2013]. Effect of tree morphometry on variability of *NSRF* with vegetation density is also significant. Taller trees, larger and denser crowns, and cylindrical shaped crowns exhibit lower net snowcover radiation on forest floor at intermediate vegetation densities and larger radiation at high vegetation densities. The optimum vegetation density at which $NSRF$ is minimum, decreases with increasing tree height, crown radius and crown density. On the other hand, larger crown depth leads to an increase in the vegetation density at which radiation is minimum [*Seyednasrollah and Kumar*, 2013].

The location-dependent variability of $NSRF$ with changing vegetation density is still unknown. Location of forests is expected to influence the variability in $NSRF$ with vegetation density by influencing both shortwave and longwave radiation components. At higher latitudes, solar altitude angle decreases thus causing shortwave radiation to decrease. Additionally, both L_{Net} and S_{Net} are affected by site-specific climatological characteristics (e.g. air temperature [*Lundquist et al.*, 2013], relative humidity [*Marthews et al.*, 2012] and cloud cover [*Flerchinger et al.*, 2009]). This paper quantifies the effects of location of forest on the magnitude of net radiation reaching the floor and its variations with changing vegetation density. Simulations are conducted for a wide range of vegetation densities using Forest Radiation Model [*Seyednasrollah et al.*, 2013], at six mid to high latitude locations in white spruce (*Picea glauca*) forests in North America. White spruce forests are widely distributed species in United States and Canada, and extend from around 43º to 69º latitude [*plantmaps.com*, 2012].

2 Model and Data

The physically-based Forest Radiation Model (FoRM) is used in this study to map the location-dependent variability of $NSRF$ with changing vegetation density. The model has the ability to simulate spatial and temporal gradients of the individual radiation components over a uniformly distributed infinite extent of trees. Although the model can calculate radiation for different tree shapes, the analysis here is restricted to cylindrical shaped white spruce trees, a widely prevalent conifer in mid-latitudes of North America. White spruce trees are widespread across northern North America (Figure 1), extending from Alaska, Yukon, and British Columbia, and continuing eastward to Nova Scotia, Newfoundland, New Brunswick, Québec, and Maine and Vermont in the northeastern United States [*plantmaps.com*, 2012; *USDA*, 2011]. White spruce can grow up to 27 meters in height and 6 meters in width [*ADF*, 2012; *MFC*, 1908]. In this analysis, a typical tree size is considered, with crown radius of 3 meters and tree height of 24 meters.

2.1 Radiation calculations in FoRM

$NSRF$ is calculated from the beginning ($t1$) to the end ($t2$) of the snow season:

$$NSRF = \frac{\int_{t1}^{t2} \int_A R_{Net}\, dA\, dt}{(t2 - t1)A}, \qquad \text{Eq. 1}$$

where A is area of forest floor control volume and R_{Net} is net radiation flux on the forest floor. R_{Net} is evaluated for a snow season that ranges from winter ($t1$) to summer ($t2$) solstices. The period conservatively overspreads the entire duration of snow season in white spruce habitat. R_{Net} is modeled as the sum of the net longwave (L_{Net}) and net shortwave (S_{Net}) energy components:

$$R_{Net} = L_{Net} + S_{Net} \qquad \text{Eq. 2}$$

L_{Net} in the model is evaluated by calculating the sum of incoming longwave emissions from tree crown ($\downarrow L_{crown}$), trunk ($\downarrow L_{trunk}$), and sky ($\downarrow L_{sky}$) and the emitted longwave radiation from snow ($\uparrow L_{snow}$) as:

$$L_{Net} = SVF\ \sigma\varepsilon_{sky}{T_{sky}}^4 + TVF\ \sigma\varepsilon_{can}{T_{trunk}}^4 + (1 - SVF - TVF)\sigma\varepsilon_{can}{T_{crown}}^4 - \sigma\varepsilon_{snow}{T_{snow}}^4 \qquad \text{Eq. 3}$$

where σ is Stefan-Boltzmann constant (σ=5.67×10^{-8} $Wm^{-2}K^{-4}$), ε_{sky}, ε_{can} and ε_{snow} are sky, canopy and snow emissivities (dimensionless) respectively, and T_{sky}, T_{crown}, T_{trunk} and T_{snow} are sky, crown, trunk and snow temperatures (K). T_{sky} is set to air temperature [*Lawler and Link*, 2011]. T_{sky} for the simulated snow season is obtained by fitting a periodic function to long term air temperature data (Table 2) from the National Climatic Data Center [*NCDC*, 2012] meteorological stations, such that both diurnal and season variations are accounted for. Snow temperature is set to the dew point temperature (T_{dp}), when T_{dp}<0 and zero otherwise [*Andreas*, 1986]. In absence of tree crown and trunk temperature data, respective temperatures are obtained by regressing the difference in observed air and crown/trunk temperatures that were presented in *Pomeroy et al.* [2009], against simulated net incident solar radiation. This assumes that the difference in canopy (crown and trunk) and air temperature is mostly driven by incident solar radiation. The emissivity of snow and canopy (both crown and trunk) are set to 1.0 [*Dozier and Warren*, 1982; *Sicart et al.*, 2006; *Warren*, 1982] and 0.98 [*Pomeroy et al.*, 2009], respectively. Sky emissivity (ε_{sky}) is evaluated using the Prata-Kimball model [*Kimball et al.*, 1982; *Prata*, 1996], which was suggested by *Flerchinger et al.* [2009] as one of the more reliable models for evaluation of sky emissivity under clear and cloudy sky conditions. Average daily cloud cover, which is used for evaluation of ε_{sky}, is obtained from the National Renewable Energy Laboratory [*NREL*, 2012] data for sites located in the United States, and the Canadian Weather Energy and Engineering Datasets [*CWEEDS*, 2013] for sites located in Canada. Other relevant meteorological variables, such as relative humidity, are obtained from NCDC data [*NCDC*, 2012]. Net shortwave radiation, S_{Net}, is evaluated by quantifying incoming direct ($\downarrow S_{dir}$), diffuse ($\downarrow S_{dif}$), and multiple reflected shortwave radiation components between snow and canopy using [*Seyednasrollah et al.*, 2013]:

$$S_{Net} = S_{extr} \left(\frac{P(\theta, Z)\,(1-\alpha_{dir})\tau_b \cos\theta}{1-\alpha_{dir}\alpha_c(1-SVF)} + \frac{SVF\,(1-\alpha_{dif})\tau_d \cos\phi\ \cos^2(\beta/2)}{1-\alpha_{dif}\alpha_c(1-SVF)} \right) \qquad \text{Eq. 4}$$

where S_{extr} is extraterrestrial radiation, α_{dir}, α_{dif} and α_c are direct, diffuse snow albedos and canopy albedo, τ_b and τ_d are atmospheric transmittance for beam and diffuse radiation, ϕ, θ and Z are solar zenith, incidence (the angle between the sun and normal to the surface) and azimuth angles respectively, SVF is local sky view factor, and P is the probability that a ray is not blocked by forest. Snow albedo has a spectral variation from 0 to 0.8 depending on snow age, grain size, and wavelength [*Warren and Wiscombe*, 1980; *Wiscombe and Warren*, 1980]. An intermediate value of 0.4, representative of the seasonal albedo for direct shortwave radiation in forested settings [*Melloh et al.*, 2002], was used in this analysis. Snow albedo for diffuse radiation, α_{dif}, is set equal to 0.8 [*Wang and Zeng*, 2010]. Canopy (crown and trunk) albedo is relatively smaller and is set to be 0.2 [*Bohren and Thorud*, 1973; *Eck and Deering*, 1990; 1992]. P is evaluated by a probabilistic ray tracing approach which accounts for the path length of the solar beam through individual canopy structures. Sky view factor, SVF, is estimated using the *SkyMap* algorithm. More details about the calculation of individual radiation components are available in *Seyednasrollah et al.* [2013] and *Seyednasrollah and Kumar* [2013].

2.2 Selected Sites

Six white spruce forest sites distributed across the United States and Canada are selected to study the variability of net radiation for different vegetation densities along a latitudinal transect (see Figure 1). The selection of sites is made based on three criteria: (a) situated in white spruce forests, (b) located in mid to high latitudes, and (c) sites should have long-term temperature records (see Table 1). Model simulations are performed for two representative snow seasons at all the six selected locations. One scenario considers a completely clear sky cover during the snow season, while other accounts for interspersed cloudy conditions based on data at respective sites. Climatological characteristics of the selected sites are shown in Table 2. Seasonal air temperature data suggests a decreasing trend in air temperature for higher latitudes. However, the site Chulitna does not follow this trend.

3 Results and Discussion

Variability of both S_{Net} and L_{Net} with vegetation density are simulated by FoRM at all the six selected sites for a range of slope angles and orientations. Vegetation density is quantified as d^{-1}, where d is the average distance between trees in an idealized uniform forest. It is to be emphasized that the model has been previously validated against the observed shortwave and longwave radiation data in a uniform lodgepole pine forest at the Local Scale Observation Site (LSOS, [*NSIDC*, 2013]) in Fraser, CO, USA [*Seyednasrollah et al.*, 2013]. By using the same configuration of forest at different locations, the role of latitudinal location and associated meteorological characteristics on variation of $NSRF$ with changing vegetation density is isolated.

3.1 Effects of Latitudinal Location and Meteorological Characteristics on Net Shortwave Radiation Reaching the Forest Floor

3.1.1. On a level forest floor: Variation of S_{Net} with vegetation density for snow seasons with completely clear or interspersed cloudy conditions In northern hemisphere, with increasing latitude, solar altitude angle decreases. As a result, the incoming shortwave radiation hits the level floor at smaller angles, resulting in reduction in net shortwave radiation. This is evident in the monotonically decreasing trend in net shortwave radiation with increase in latitude, at all considered vegetation densities in clear sky conditions (Figure 2-a). On the other hand, for snow seasons with interspersed cloudy sky conditions, comparative differences in S_{Net} between locations are also influenced by differences in sky cover and its seasonal variation at the study sites. With increasing sky cloudiness, the incoming direct shortwave radiation declines [*Liu and Jordan*, 1960], whereas the diffuse portion of shortwave radiation increases because of enhanced scattering [*Monteith and Unsworth*, 2008]. Since the decrease in direct radiation is generally much more than the increase in the diffuse component, S_{Net} decreases with increase in cloud cover [*Campbell*, 1985]. As a result, all study sites were observed to receive less amount of shortwave radiation in interspersed cloudy sky conditions than in clear sky conditions. The decrease in shortwave radiation is generally observed to be proportional to sky cloud fraction, which translates to larger decrease in S_{Net} for sites with larger cloud fraction. However, the variation of S_{Net} with sky cloudiness is not always linear, as the magnitude of decrease in S_{Net} with sky cloudiness is also influenced by site elevation, local atmospheric turbidity, aerosols concentration, temporal variation of sky cloudiness over the season and uncertainties associated with the sources of data. For instance, S_{Net} at Greenville (C≈56%) declines to about 61% of its magnitude in clear sky conditions; while at Prince Albert (C≈53%), S_{Net} reduces to about 80%

of its magnitude in clear sky conditions. Additionally, because of the influence of multiple controls during interspersed cloudy sky conditions, S_{Net} does not always show a monotonic trend with either latitude or sky cover fraction. For example, in open areas to low vegetation densities (d^{-1} < 0.04 m^{-1}) where direct shortwave radiation is the dominant shortwave component, the largest shortwave radiation is observed at Prince Albert (C≈53%) followed by Buffalo Narrows (C≈53%), the two locations that exist at relatively low latitudes and also where sky cover fraction is relatively small. Net shortwave radiation was observed to be less in Greenville (C≈56%) and Trout Lake (C≈51%) than in Buffalo Narrows. In contrast, the two high latitude sites, Indian Mountains and Chulitna, with high seasonal cloud cover (C≈68-69%) expressed the smallest net shortwave radiation for all considered vegetation densities (Figure 2-b). For intermediate to high vegetation densities (0.04m^{-1} < d^{-1} < 0.13m^{-1}) where the diffuse radiation gradually becomes the principal portion of net shortwave radiation reaching the forest floor, the decrease in $\downarrow S_{dir}$ with sky cover is balanced out by the increase in $\downarrow S_{dif}$. As a result, trend of S_{Net} with latitude at these vegetation densities follows the same trend that exist in snow seasons with completely clear sky conditions, with largest magnitude observed at Greenville, followed by Prince Albert, Buffalo Narrows, Trout Lake, and Chulitna and Indian Mountains, respectively. In very high vegetation densities (d^{-1}>0.13m^{-1}), S_{Net} becomes very small at all study sites with no significant difference between locations.

3.1.2. On a sloping forest floor: Variation of S_{Net} with vegetation density for snow seasons with completely clear or interspersed cloudy conditions Latitudinal influence on variation of net radiation with vegetation density changes with slope angle and aspect of the forested hillslope. S_{Net} on a inclined hillslope shows a similar trend in its variability across different locations as is expressed in level forests for clear sky conditions (see Figure 3-a). The only marked difference in the shortwave radiation regime on inclined slopes, with respect to level forests, is the increase in magnitude of direct shortwave radiation with slope angle for south-facing slopes, especially at lower vegetation densities. This is mainly due to: (a) the decrease in solar incidence angle (the angle between the sun and normal to the surface) and (b) the decrease in shading fraction for steeper hillslopes [*Seyednasrollah et al.*, 2013]. Along similar lines, changes in the orientation of the hillslope from south-facing to north-facing reduces S_{Net}, because of a continuous increase in solar incidence angle and shading fraction for north-ward slopes. The decrease in shortwave radiation is much more at lower vegetation densities, where direct shortwave radiation is relatively significant than at higher vegetation densities. For snow season with interspersed cloudy sky conditions (Figure 3-b), the increase in S_{Net} with slope angle on south facing slopes is larger at sites with smaller seasonal sky cover. On north-facing hillslopes with interspersed cloudy sky conditions in the snow season, the decrease in S_{Net} with slope angle is also larger at sites with smaller seasonal sky cover (Prince Albert, Buffalo Narrows and Trout Lake; see Figure 3-b).

3.2 Effects of Latitudinal Location and Meteorological Characteristics on Net Longwave Radiation Reaching the Forest Floor

3.2.1. On a level forest floor: Variation of L_{Net} with vegetation density for snow seasons with completely clear or interspersed cloudy conditions Longwave radiation reaching the forest floor is affected by changes in vegetation density because of change in sky and trunk view factor. Of the four longwave radiation components, $\uparrow L_{snow}$ is independent of sky view factor and vegetation density (Eq. 3). Canopy emissivity, $\downarrow L_{can}$, which is evaluated as $\downarrow L_{crown} + \downarrow L_{trunk}$, is higher than clear sky emissivity and therefore the variation of net longwave radiation with changing sky view factor is dominated by $\downarrow L_{can}$. As a result, L_{Net} varies conversely with SVF, and hence it increases with increasing vegetation density at all the six study sites (Figure 4-a and b). However, at any particular vegetation density, net longwave radiation does not show a monotonic variation with latitude, in part because of variations in cloud cover, relative humidity, and air, crown, trunk and snow temperatures, which influence L_{Net} directly or indirectly. Notably, monotonic trend in L_{Net} is not expressed even for clear sky conditions. This is also true for stations (e.g. Greenville, Prince Albert, Trout Lake and Indian Mountains) for which mean snow-season air temperature varies inversely with latitude (Figure 4-a, inset). The variation of L_{Net} at different sites is highly nonlinear. At low vegetation densities (SVF → 1), the trend in L_{Net} is determined by $\sigma(\varepsilon_{sky}{T_{sky}}^4 - \varepsilon_{snow}{T_{snow}}^4)$ based on Eq. 3. Depending on the frequency of how often dew point temperatures are above zero degree Celsius and the magnitude of snow and clear sky emissivity, the difference between incoming sky longwave radiation and outgoing longwave radiation from snow changes from location to location, resulting in the expressed variations (Figure 4-a). As a result, for open areas (SVF = 1) in clear sky conditions, L_{Net} is the smallest for Chulitna and the largest for Indian Mountains. Other four sites in the order of increasing L_{Net} are: Trout Lake, Prince Albert, Greenville and Buffalo Narrows. In contrast, for very dense forests (SVF → 0), L_{Net}, which is equal to $\sigma(\varepsilon_{can}((1 - TVF){T_{crown}}^4 + TVF\,{T_{trunk}}^4)\varepsilon_{can}{T_{can}}^4 - \varepsilon_{snow}{T_{snow}}^4)$, increases from Chulitna to Trout Lake, Indian Mountains, Prince Albert, Buffalo Narrows and Greenville (Figure 4). At intermediate vegetation densities, the ordering of sites changes based on the site specific emissivities and the temperature data. Notably, the range of L_{Net} for the vegetation densities considered here is only about 7 Wm^{-2} to 8 Wm^{-2}, for the latitudinal range considered (~45º N to ~66º N).

In addition to air temperature, sky cover fraction also plays an important role in variation of net longwave radiation component across the study sites. With increasing cloud cover, sky emissivity increases, resulting in an increase in $\downarrow L_{sky}$. On the contrary, shortwave radiation decreases with increasing sky cloudiness, leading to a decline in crown and trunk temperatures and hence a decrease in $\downarrow L_{crown}$ and $\downarrow L_{trunk}$, particularly in low vegetation densities. However the effect of sky cloudiness on $\downarrow L_{crown}$ and $\downarrow L_{trunk}$ is smaller than that on longwave radiation from sky, resulting in an increase in L_{Net} with increase in cloud cover. Because of a larger role of $\downarrow L_{sky}$ at sparse densities, the increase in L_{Net} at these vegetation densities is more than in dense forests. As a result, L_{Net} in open areas is more sensitive to sky cloudiness than in very dense forests. For interspersed cloudy sky conditions, net longwave radiation in open areas increases from Trout Lake to Prince Albert, Buffalo Narrows, Greenville and Indian Mountains (Figure 4-b) in direct proportion with seasonal average cloud cover. However due to the warm snow season, Chulitna was observed as an outlier between Prince Albert and Buffalo Narrows.

3.2.2. On a sloping forest floor: Variation of L_{Net} with vegetation density for snow seasons with completely clear or interspersed cloudy conditions Net longwave radiation does not change significantly with increasing slope angle. However, because of very modest changes in sky view factor with slope angle [*Seyednasrollah et al.*, 2013], L_{Net} is affected a little by changes in slope angle. On south-facing hillslopes, as slope angle increases, the angles subtended by southern (and lower) and northern (and higher) trees increases and decreases, respectively. Since the rate of increase of subtended angle by southern trees is large, sky view factor decreases with increasing slope angle. Following the sky view factor, L_{Net} increases a bit with increasing slope at the study locations, for both clear and interspersed cloudy sky conditions. Changes in the aspect of the hillslope toward the north reduce incoming solar radiation to the forests, causing a decrease in crown/trunk temperature, and hence a minor decrease in L_{Net}. The changes in L_{Net} with aspect are even less in interspersed cloudy sky conditions than in clear sky conditions. It is to be noted that with changes in slope and aspect, the variation of S_{Net} is far larger than in L_{Net} [*Seyednasrollah et al.*, 2013], therefore the variability of net radiation ($NSRF$) with aspect and slope is mainly influenced by changes in the shortwave component.

3.3 Net Radiation Variability

The variations of net radiation with vegetation density for clear and interspersed cloudy sky conditions in level forests are plotted in Figure 5-a and Figure 5-b, respectively.

3.3.1. On a level forest floor: Variation of $NSRF$ with vegetation density for snow seasons with completely clear or interspersed cloudy conditions For clear sky conditions in sparse vegetation densities (d^{-1}<0.08m^{-1}), the magnitude of decrease in net shortwave radiation with increasing latitude is larger than the changes in net longwave radiation at five out of six study sites (Greenville, Prince Albert, Buffalo Narrows, Trout Lake and Indian Mountains). As a result, $NSRF$ follows the variation of S_{Net} and decreases with increasing latitudes (Figure 5-a). However, $NSRF$ at Chulitna falls out of this sequence and has the smallest $NSRF$, even smaller than at Indian Mountains, which is located further north. This is because the difference in net longwave radiation between Indian Mountains and Chulitna is much more than the difference in shortwave radiation. In contrast, due to relatively smaller contribution of shortwave radiation in dense forests (d^{-1}>0.12m^{-1}), the magnitude of $NSRF$ follows the trend of longwave radiation as is expressed in Figure 4-a. As such, $NSRF$ is largest for Greenville and smallest for Chulitna in dense forests. The changing relative contributions of individual radiation components at different densities also result in differences in variability of $NSRF$ with vegetation density at different latitudes. For example, for lower latitude sites (e.g. Greenville, Prince Albert and Buffalo Narrows), where net shortwave radiation component is larger than net longwave component, $NSRF$ is generally larger for low vegetation densities or open areas with respect to dense forests. On the other hand, for higher latitude sites (e.g. Indian Mountains and Chulitna) where net longwave is dominant, $NSRF$ in very dense forests is larger than in open areas or sparse forests. The range of variation in $NSRF$ also varies across the sites. Notably, the standard deviation of net radiation (σ_{NSRF}) across different vegetation densities first decreases with latitude from Greenville (σ_{NSRF}=12.3 Wm^{-2}) to Prince Albert (σ_{NSRF}=6.4 Wm^{-2}), Buffalo Narrows (σ_{NSRF}=4.7 Wm^{-2}) and Trout Lake (σ_{NSRF}=3.7 Wm^{-2}) and then increases with latitude for Chulitna (σ_{NSRF}=3.9 Wm^{-2}) and Indian Mountains (σ_{NSRF}=4.5 Wm^{-2}). This is because in lower latitudes, the difference in net radiation between open areas and very dense forests first decreases and then increases with increasing latitude. Vegetation density at which maximum net radiation is expressed is also found to vary across the six sites. The results show that in clear sky conditions, the maximum net radiation ($NSRF_{max}$) for level forest occurs at sparser density (d_{max}^{-1}≈0.02m^{-1}) for lower latitudes areas (Greenville, Prince Albert, Buffalo Narrows and Trout Lake) and in very dense forests (d_{max}^{-1}≈0.17m^{-1}) for higher latitude sites (Indian Mountains and Chulitna). $NSRF_{max}$ varies from 23.3 Wm^{-2} to 58.2 Wm^{-2} across the six locations. Moreover, $NSRF$ at different locations often expresses a local minimum for intermediate vegetation densities. The density at which $NSRF$ is minimum (d_{min}^{-1}) decreases with increasing latitude from d_{min}^{-1}≈0.12 m^{-1} at Greenville (latitude = 45.5 ºN) to d_{min}^{-1}≈0.08m^{-1} at Indian Mountains (latitude = 66.0 ºN). $NSRF_{min}$ varies from 10.4 Wm^{-2} to 27.7 Wm^{-2} across the six locations.

For the scenario when interspersed cloudy sky conditions in snow season is considered, $NSRF$ monotonically increases with vegetation density for sites with higher cloud cover (e.g. Greenville, Indian Mountains and Chulitna; see Figure 5-b), as the shortwave component is small, and hence the longwave radiation determines the trend at all vegetation densities. This variation becomes non-monotonic for sites with lower cloud cover (e.g. Prince Albert, Buffalo Narrows and Trout Lake; see Figure 5-b), as the shortwave radiation is not too small especially in sparse forests. Unlike the scenario with completely clear sky conditions in snow season, for interspersed cloudy sky conditions, due to differences in cloud cover fraction, $NSRF$ expresses a non-monotonic trend with latitude at most vegetation densities. In open areas and sparse forests, $NSRF$ is the largest for Prince Albert, followed by Buffalo Narrows, Greenville, Trout Lake, Indian Mountains and Chulitna. However, in very dense forests, the contribution of the shortwave radiation and the incoming longwave radiation from sky are small and hence the $NSRF$'s trend with latitude in interspersed cloudy sky conditions is the same as in clear sky conditions. The range of variation in $NSRF$ is smaller at lower latitude sites (e.g. Greenville, Prince Albert and Buffalo Narrows) than at higher latitude sites (e.g. Chulitna and Indian Mountains). This is because at higher latitudes, the difference in net radiation between open areas and very dense forests is large due to smaller contribution from S_{Net}, especially at sparse densities. Because of relatively modest contribution of S_{Net} on $NSRF$, $NSRF$ is generally the largest in dense forests at five out of six considered sites. $NSRF_{max}$ varies from 23.8 Wm^{-2} to 31.2 Wm^{-2} across the six locations. $NSRF_{min}$ shows a much wider variation across the six sites, with maximum and minimum $NSRF_{min}$ being equal to 1.1 Wm^{-2} and 23.4 Wm^{-2} respectively. The density at which $NSRF$ is minimum (d_{min}^{-1}) generally increases with decreasing latitude from d_{min}^{-1}≈0.01 m^{-1} at Indian Mountains (latitude = 66.0 ºN) to d_{min}^{-1}≈0.085m^{-1} at Prince Albert (latitude = 53.2 ºN). Greenville (latitude = 45.5 ºN) is exception to this trend, as $NSRF_{min}$ is again expressed in very sparser forests at the site.

3.3.2. On a sloping forest floor: Variation of NSRF with vegetation density for snow seasons with completely clear or interspersed cloudy conditions The trend of $NSRF$ with vegetation density changes with both slope and aspect. For south-facing hillslopes in clear sky conditions, S_{Net} and hence $NSRF$ increases with increasing slope angle, resulting in an increase in d_{min}^{-1} at all locations (Figure 6). The changes in $NSRF$ with slope angle are larger in sparse forests than in dense forests. In relatively dense forests (d^{-1}>0.12 m^{-1}), the changes in net shortwave and longwave components cancel each other out, and hence $NSRF$ becomes less sensitive to vegetation density, particularly for higher slopes where the rate of changes in longwave and shortwave components are equal (slope≥30°). Similar to level forests, maximum $NSRF$ is observed in relatively sparse forests (d_{max}^{-1}≈0.02-0.03m^{-1}) for all south-facing slopes. Compared to level forests in mid- to high-latitude sites, for which the magnitude of $NSRF_{min}$ to net radiation in open areas ($NSRF_{open}$) increases with increasing site's latitude (from 48% in Greenville to 82% in Indian Mountains, see Table 3), this fraction for south-facing hillslopes (slope=15°) varies from 40% in Greenville to 65% in Indian Mountains (see Table 4). In contrast, the fraction of $NSRF_{min}$ to net radiation in very dense forest ($NSRF_{dense}$) at different sites show a decreasing trend from 90% to 47% in level forests (Table 3) and 95% to 70% for a 15° south-facing hillslope (Table 4).

Differences in aspect of forested hillslopes also cause variability in the trend of $NSRF$ with vegetation density and latitude. With aspect of the hillslope changing from south to east/west and then to north in clear sky conditions, L_{Net} remains almost constant (a minor change is experienced due to changes in tree crown and trunk temperatures with changes in insolation) while S_{Net} decreases, resulting in a decrease in $NSRF$. The rate of decrease in $NSRF$ with aspect is stronger in open areas with respect to dense forests. As a result, L_{Net} gradually becomes the dominant component for north-facing aspects; and hence, $NSRF$ is more likely to follow an increasing trend with increasing vegetation density. For example, non-monotonic variability of

$NSRF$ with vegetation density at high latitude sites become strictly monotonically increasing for north facing slopes (Figure 6, leftmost column). Aspect also affects the influence of variation of $NSRF$ with vegetation density. Since increase in slope angle leads to increase/decrease in S_{Net} on south/north facing slopes, especially at lower vegetation densities, $NSRF$ shows a stronger decreasing/increasing trend for south/north facing hillslopes at larger slope angles. This is distinctly apparent on north facing slopes for which $NSRF$ is monotonically increasing for two out of six location on a 15º slope but increases monotonically at all six locations on a 45º slope. Similarly, on south facing hillslopes with slope=15º, the minimum radiation occurs at intermediate densities for five out of six study locations (Prince Albert, Buffalo Narrows, Trout Lake, Chulitna, Indian Mountains), however, the minimum radiation for slopes=45º, occur in very dense forest at all six considered sites because of a decreasing trend in $NSRF$ (see Figure 6). Since L_{Net} shows only mild variations with latitude, forests with steeper slopes on north-facing aspects are less sensitive to changes in latitudinal location with respect to forests with south-facing aspects and on lower slopes.

For scenarios with interspersed cloudy sky conditions in snow season, in very sparse vegetation densities on south-facing slopes (e.g. slope=15º in Figure 7), Prince Albert and Buffalo Narrows show largest $NSRF$s among the study locations, due to large shortwave contribution. $NSRF$ decreases from Greenville to Trout Lake, Indian Mountains and Chulitna. For south-facing slopes, the existence of a minimum net radiation at intermediate densities was observed at four out of six study locations (Greenville, Prince Albert, Buffalo Narrows and Trout Lake). Because of the increase in S_{Net}, the minimum shifts toward dense forests with increasing slope angle at these sites. Since longwave radiation dominantly controls $NSRF$ at high latitude sites (e.g. Chulitna and Indian Mountains; see Figure 7), $NSRF$ shows a steady increasing trend with vegetation density for all slopes and aspects at high latitudes. With changing aspect of the sites towards north, shortwave radiation contribution becomes marginal (see Figure 6); and hence, the variability of $NSRF$ with vegetation density becomes monotonically increasing with little sensitivity to site location. As a result, for northern aspects, $NSRF$ is maximum in dense forests.

4 Summary and Conclusion

The study illustrates the role of latitudinal location of the forest and associated metrological conditions on the magnitude and variability of net radiation on snow-covered forest floor, for a range of vegetation densities, slopes and aspects. The results in level forests for clear sky conditions showed that the rate of decrease in net shortwave radiation with increasing latitude is greater than changes in net longwave radiation caused by temperature drop. As a result, the variability of net radiation with latitude at locations with vegetation density less than 0.04 m^{-1} are controlled by shortwave radiation, while in denser forests (density ≥ 0.14 m^{-1}) the variation is dominated by longwave radiation trend, which in turn is dominantly influenced by site temperature. Variation of net radiation with latitude in forests with intermediate densities (0.04 m^{-1}<d^{-1}<0.14 m^{-1}) are controlled by both shortwave and longwave radiation components (see Figure 5). Minimum net radiation is more likely to occur at lower vegetation densities for sites at higher latitudes. For the considered sites, the minimum net radiation occurs at intermediate densities from 0.08 m^{-1} to 0.12 m^{-1}. The range of variation in net radiation between open areas and very dense forests, however, first decreases and then increases with increasing latitude. Sky cloudiness affects the variations in net radiation with vegetation at all locations by markedly reducing shortwave radiation, especially in sparse forests. As a result, for snow seasons with interspersed cloudy sky conditions, shortwave radiation is no longer the dominant energy component (even in very sparse forests) and longwave radiation becomes the dominant component for a wider range of vegetation densities (d^{-1}>0.13 m^{-1}) than in clear sky conditions (Figure 5-b). Since the variability of longwave radiation across different locations is small, net radiation is only mildly sensitive to site location in very dense forests (d^{-1}>0.14 m^{-1}), for both clear and interspersed cloudy sky conditions. In these regions, site temperature data (temperature magnitude and its temporality) plays the main role in magnitude of net radiation reaching the forest floor. In spite of aforementioned changes in radiation contributions due to interspersed sky cover, the density at which radiation is minimum still generally increases with decreasing latitude. Notably, the range of net radiation across the six sites is relatively small for a wide range of vegetation densities in interspersed cloudy snow season.

The obtained results also explain how net radiation and its variability with vegetation density vary with changes in site topographical characteristics (slope and aspect), in mid- to high- latitude forests. On south-facing forested hillslopes, the shortwave radiation remains the primary radiation component in regions with vegetation density less than 0.05 m^{-1}, while the longwave component is the dominant control in areas with vegetation density larger than 0.13 m^{-1}. As aspect of forested hillslope changes from south-facing to north-facing, the shortwave-dominant region becomes narrower, with vegetation density less than 0.02 m^{-1} for clear sky conditions. Longwave radiation, on the other hand, becomes dominant for a wider range of vegetation densities (d^{-1}>0.12 m^{-1}), particularly in higher slopes (see Figure 6). The changing contribution of radiation components on south facing hillslopes results in vegetation density at which radiation is minimum (d_{min}^{-1}) to increase with slope angle at all locations. However, the trend is opposite for north facing aspects where with increase in slope angle, minimum radiation is obtained at smaller densities. In interspersed cloudy sky conditions, longwave radiation and hence site climatological characteristics become the main contributing components for a wider range of vegetation densities (d^{-1}>0.11 m^{-1}) with changing the slope and aspect toward the north. Notably, only south-facing mid-latitude sites with relatively low cloud cover exhibit a non-monotonic $NSRF$ with changing vegetation density. Other site conditions result in a monotonically increasing radiation with increasing vegetation density. The range of net radiation across the six sites in interspersed cloudy snow season is relatively smaller than in clear sky conditions, for all slope angles and aspects. In spite of these changes in radiation contributions due to interspersed sky cover, the density at which radiation is minimum still generally increases with decreasing latitude on south facing slopes. On north facing slopes however, because of longwave dominance at all densities, net radiation is minimum in open areas and very sparse forests.

These results suggest that occurrence of a radiation minimum, the density at which it happens, the range of variation in radiation with vegetation density, and dominance of individual radiation components depends on the location, climate, slope and aspect of the site. The location based dependencies on net snow cover radiation have implications on prioritization of observation resources, parameterizations of water and energy fluxes and in forest management. Based on the latitudinal, topographic and meteorological configurations, one can decide on which radiation component between longwave or shortwave measurements should be first made. Presented results regarding the role of density of vegetation in determining net snow cover radiation, and how the said relationship is a function of latitudinal controls and associated meteorological characteristics, may guide future work to include a vegetation density dependent water balance and energy parameterization in coarse scale models (e.g. Community Earth

System Model, CESM). Results could also be used for quantification of the uncertainties in energy and melt estimation. The results could be applied to support optimal forest management practices to obtain the desired net radiation and hence melt regime on the forest floor by altering vegetation densities. At locations where stocking/thinning of trees has to be undertaken, density could be managed to achieve the minimum radiation, which as the results show will happen at sparser densities in high-latitude forests. The monotonically increasing trend of net radiation with vegetation density at all six selected sites on north-facing hillslopes indicates that thinning of trees can be performed to minimize the snowmelt rate for a wide range of locations. In contrast, planting of trees in large gaps to increase the density of trees could also be used as an effective strategy to reduce net radiation, and hence the melt rate, on south-facing hillslopes in mid-latitude areas. The results also suggest that the largest potential for reduction in energy through forest management is on south facing hillslopes at lower latitudes. However, the reduction in energy is expected to be relatively muted with increasing cloud cover.

Acknowledgments

Data sets used in the paper are freely available to public from National Climatic Data Center (www.ncdc.noaa.gov), National Renewable Energy Laboratory (www.nrel.gov) and Canadian Weather Energy and Engineering Datasets (weather.gc.ca).

5 References

ADF (2012), ArborDayFoundation-Tree Details—The Tree Guide at arborday.org, edited, Arbor Day Foundation, http://www.arborday.org/.

Aguado, E. (1985), Radiation Balances of Melting Snow Covers at an Open Site in the Central Sierra-Nevada, California, *Water Resour Res*, *21*(11), 1649-1654.

Andreas, E. L. (1986), A New Method of Measuring the Snow-Surface Temperature, *Cold Reg Sci Technol*, *12*(2), 139-156.

Bohren, C. F., and D. B. Thorud (1973), 2 Theoretical Models of Radiation Heat-Transfer between Forest Trees and Snowpacks, *Agr Meteorol*, *11*(1), 3-16.

Campbell, G. S. (1985), *Soil physics with BASIC : transport models for soil-plant systems*, xvi, 150 p. pp., Elsevier, Amsterdam ; New York.

CWEEDS (2013), Canadian Weather Energy and Engineering Datasets, edited, http://weather.gc.ca/.

Dozier, J., and S. G. Warren (1982), Effect of Viewing Angle on the Infrared Brightness Temperature of Snow, *Water Resour Res*, *18*(5), 1424-1434.

Eck, T. F., and D. W. Deering (1990), Canopy Albedo and Transmittance in a Boreal Forest, *Remote Sensing Science for the Nineties, Vols 1-3*, 883-886.

Eck, T. F., and D. W. Deering (1992), Canopy Albedo and Transmittance in a Spruce-Hemlock Forest in Mid-September, *Agr Forest Meteorol*, *59*(3-4), 237-248.

Elder, K., J. Dozier, and J. Michaelsen (1991), Snow Accumulation and Distribution in an Alpine Watershed, *Water Resour Res*, *27*(7), 1541-1552.

Flerchinger, G. N., W. Xaio, D. Marks, T. J. Sauer, and Q. Yu (2009), Comparison of algorithms for incoming atmospheric long-wave radiation, *Water Resour Res*, *45*.

Kimball, B. A., S. B. Idso, and J. K. Aase (1982), A Model of Thermal-Radiation from Partly Cloudy and Overcast Skies, *Water Resour Res*, *18*(4), 931-936.

Lawler, R. R., and T. E. Link (2011), Quantification of incoming all-wave radiation in discontinuous forest canopies with application to snowmelt prediction, *Hydrol Process*, *25*(21), 3322-3331.

Liu, B. Y. H., and R. C. Jordan (1960), The Interrelationship and Characteristic Distribution of Direct, Diffuse and Total Solar Radiation, *Sol Energy*, *4*(3), 1-19.

Lundquist, J. D., S. E. Dickerson-Lange, J. A. Lutz, and N. C. Cristea (2013), Temperature-induced tipping point in net effect of forests on snowmelt, *Water Resour Res*, *under review*.

Marthews, T. R., Y. Malhi, and H. Iwata (2012), Calculating downward longwave radiation under clear and cloudy conditions over a tropical lowland forest site: an evaluation of model schemes for hourly data, *Theor Appl Climatol*, *107*(3-4), 461-477.

Melloh, R. A., J. P. Hardy, R. N. Bailey, and T. J. Hall (2002), An efficient snow albedo model for the open and sub-canopy, *Hydrol Process*, *16*(18), 3571-3584.

MFC (1908), Forest trees of Maine edited, p. v., Augusta.

Monteith, J. L., and M. H. Unsworth (2008), *Principles of environmental physics*, 3rd ed., xxi, 418 p. pp., Elsevier ;, Amsterdam ; Boston.

NCDC (2012), edited, http://www.ncdc.noaa.gov/oa/ncdc.html, Accessed July, 2012.

NREL (2012), National Renewable Energy Laboratory, edited, www.nrel.gov. Accessed February 2013.

NSIDC, N. S. a. I. D. C. (2013), The Cold Land Processes Field Experiment, edited, The Cold Land Processes Field Experiment, http://nsidc.org/data/clpx/clpx_data.html.

plantmaps.com (2012), PlantMaps-Picea glauca - white spruce Interactive Native Range Distribution Map with USDA Hardiness Zones., edited, http://www.plantmaps.com/nrm/picea-glauca-white-spruce-native-range-map.php.

Pomeroy, J. W., D. Marks, T. Link, C. Ellis, J. Hardy, A. Rowlands, and R. Granger (2009), The impact of coniferous forest temperature on incoming longwave radiation to melting snow, *Hydrol Process*, *23*(17), 2513-2525.

Prata, A. J. (1996), A new long-wave formula for estimating downward clear-sky radiation at the surface, *Q J Roy Meteor Soc*, *122*(533), 1127-1151.

Price, A. G. (1988), Prediction of Snowmelt Rates in a Deciduous Forest, *J Hydrol*, *101*(1-4), 145-157.

Reifsnyder, W. E., and H. W. Lull (1965), *Radiant energy in relation to forests*, vi, 111 p. pp., U.S. Dept. of Agriculture, Forest Service ; For sale by the Superintendent of Documents, U.S. Govt. Print. Off., Washington,.

Seyednasrollah, B., and M. Kumar (2013), Effects of tree morphometry on net snow cover radiation on forest floor for varying vegetation densities, *Journal of Geophysical Research: Atmospheres*, *118*(22), 2012JD019378.

Seyednasrollah, B., M. Kumar, and T. E. Link (2013), On the role of vegetation density on net snow cover radiation at the forest floor, *J Geophys Res-Atmos*, *118*(15), 8359-8374.

Sicart, J. E., J. W. Pomeroy, R. L. H. Essery, and D. Bewley (2006), Incoming longwave radiation to melting snow: observations, sensitivity and estimation in northern environments, *Hydrol Process*, *20*(17), 3697-3708.

USACE (1956), *Snow hydrology; summary report of the snow investigations*, xxv, 437 p. pp., North Pacific Division, Corps of Engineers, U.S. Army, Portland, Or.,.

USDA, N. (2011), Plant Guide, White Spruce, Picea glauca (Moench) Voss, edited, http://plants.usda.gov/plantguide/pdf/pg_pigl.pdf.

Wang, Z., and X. B. Zeng (2010), Evaluation of Snow Albedo in Land Models for Weather and Climate Studies, *J Appl Meteorol Clim*, *49*(3), 363-380.

Warren, S. G. (1982), Optical-Properties of Snow, *Rev Geophys*, *20*(1), 67-89.

Warren, S. G., and W. J. Wiscombe (1980), A Model for the Spectral Albedo of Snow .2. Snow Containing Atmospheric Aerosols, *J Atmos Sci*, *37*(12), 2734-2745.

Wiscombe, W. J., and S. G. Warren (1980), A Model for the Spectral Albedo of Snow .1. Pure Snow, *J Atmos Sci*, *37*(12), 2712-2733.

Tables:

Table 1. Geography of the study sites

Table 2. Climatological characteristics of the study sites

Table 3. Minimum and maximum net radiation compared to radiation in open ($NSRF_{open}$) and very dense ($NSRF_{dense}$) areas for level forests at different locations

Table 4. Minimum and maximum net radiation compared to radiation in open ($NSRF_{open}$) and very dense ($NSRF_{dense}$) areas for south-facing forests with slope=15º at different locations

Figures:

Figure 1. Spatial distribution of white spruce in North America. The six locations considered for analyses (see Table 1) are also identified (image has been modified based on the original map from www.usgs.gov).

Figure 2. Variations of net shortwave radiation on level forests with vegetation density at different sites in: (a) clear and (b) interspersed cloudy sky conditions. Legend lists the sites in increasing order of latitude from top to bottom.

Figure 3. Variations of net shortwave radiation with vegetation density at different sites for different slope angle and aspect of the forested hillslope in: (a) clear and (b) interspersed cloudy sky conditions. Legend lists the sites in increasing order of latitude from top to bottom.

Figure 4. Variations of net longwave radiation on level forests with vegetation density at different sites in: (a) clear (inset: seasonal average air temperature), and (b) interspersed cloudy sky conditions. Legend lists the sites in increasing order of latitude from top to bottom.

Figure 5. Variations of net radiation on level forests with vegetation density at different sites in: (a) clear and (b) interspersed cloudy sky conditions. Sites are listed in increasing order of latitude. The red and green bands indicate the vegetation densities for which shortwave ($\Delta S_{Net}/\Delta L_{Net}$>5) and longwave ($\Delta L_{Net}/\Delta S_{Net}$>5) radiation components dominantly control the variation with latitude, respectively. Δ denotes the range of respective energy component across all six sites.

Figure 6. Variations of net radiation with vegetation density at different sites for different slope angles and aspects of the forested hillslope in clear sky conditions. Sites are listed in increasing

order of latitude. The red and green bands indicate the vegetation densities for which shortwave ($\Delta S_{Net}/\Delta L_{Net}$>5) and longwave ($\Delta L_{Net}/\Delta S_{Net}$>5) radiation components dominantly control the variation with latitude, respectively. Δ denotes the range of respective energy component across all six sites.

Figure 7. Variations of net radiation with vegetation density at different sites for different slope angles and aspects of the forested hillslope in interspersed cloudy sky conditions. Sites are listed in increasing order of latitude. The red and green bands indicate the vegetation densities for which shortwave ($\Delta S_{Net}/\Delta L_{Net}$>5) and longwave ($\Delta L_{Net}/\Delta S_{Net}$>5) radiation components dominantly control the variation with latitude, respectively. Δ denotes the range of respective energy component across all six sites.

Table 1. Geography of the study sites

Site	NCDC code	Latitude (ºN)	Longitude (ºW)	Elevation (m)
Greenville, ME, USA	KGNR	45.5	69.6	423
Prince Albert, SK, Canada	CYPA	53.2	105.7	428
Buffalo Narrows, SK, Canada	CYVT	55.8	108.4	440
Trout Lake, BC, Canada	CWTE	60.4	121.2	498
Chulitna, AK, USA	PAEC	62.8	149.9	411.5
Indian Mountains, AK, USA	PAIM	66.0	153.7	388.9

Table 2. Climatological characteristics of the study sites

Site	Observation period	Seasonal average air temperature (ºC)	Seasonal cloud cover (%)
Greenville	1982-2012	-1.2	56
Prince Albert	1955-2012	-4.8	53
Buffalo Narrows	1979-2012	-4.5	53
Trout Lake	1994-2012	-8.5	51
Chulitna	2006-2012	-3.4	68
Indian Mountains	2005-2012	-9.3	69

Table 3. Minimum and maximum net radiation compared to radiation in open ($NSRF_{open}$) and very dense ($NSRF_{dense}$) areas for level forests at different locations

Sky condition	Site	d_{min}^{-1} (m^{-1})	$NSRF_{min}$ (Wm^{-2})	d_{max}^{-1} (m^{-1})	$NSRF_{max}$ (Wm^{-2})	$NSRF_{open}$ (Wm^{-2})	$NSRF_{dense}$ (Wm^{-2})
Clear sky	Greenville	0.12	27.7	0.02	58.2	56.9	30.8
	Prince Albert	0.11	21.5	0.02	38.7	37.1	27.6
	Buffalo Narrows	0.1	21.1	0.02	34.4	32.7	28.7
	Trout Lake	0.09	13.6	0.02	23.8	22.1	23.6
	Chulitna	0.08	10.4	0.17	23.3	14	23.3
	Indian Mountains	0.08	12.7	0.17	26.9	15.4	26.9
Interspersed cloudy sky	Greenville	0.01	23.4	0.17	31.2	23.4	31.2
	Prince Albert	0.09	21.5	0.17	28.1	26.7	28.1
	Buffalo Narrows	0.08	21.2	0.17	29.1	25	29.1
	Trout Lake	0.07	13.3	0.17	24	15.3	24
	Chulitna	0.01	1.1	0.17	23.8	1.1	23.8
	Indian Mountains	0.01	5.9	0.17	27.3	5.9	27.3

Table 4. Minimum and maximum net radiation compared to radiation in open ($NSRF_{open}$) and very dense ($NSRF_{dense}$) areas for south-facing forests with slope=15º at different locations

Sky condition	Site	d_{min}^{-1} (m^{-1})	$NSRF_{min}$ (Wm^{-2})	d_{max}^{-1} (m^{-1})	$NSRF_{max}$ (Wm^{-2})	$NSRF_{open}$ (Wm^{-2})	$NSRF_{dense}$ (Wm^{-2})
Clear sky	Greenville	0.13	29.7	0.02	75	73.5	31.1
	Prince Albert	0.12	24.8	0.02	55.9	54.1	28.1
	Buffalo Narrows	0.12	25.2	0.02	51.6	49.6	29.1
	Trout Lake	0.11	18.6	0.02	40.2	38.3	24
	Chulitna	0.11	16.5	0.03	32.1	29.3	23.6
	Indian Mountains	0.1	19.1	0.03	31.9	29.1	27.2
Interspersed cloudy sky	Greenville	0.11	27.4	0.04	33.6	30.9	31.4
	Prince Albert	0.11	24.5	0.02	38.7	37.5	28.4
	Buffalo Narrows	0.11	24.9	0.02	37.4	36.2	29.4
	Trout Lake	0.1	18.2	0.03	27.5	26	24.2
	Chulitna	0.01	6.1	0.17	24	6.1	24
	Indian Mountains	0.01	10.3	0.17	27.5	10.3	27.5

Figure 1. Spatial distribution of white spruce in North America. The six locations considered for analyses (see Table 1) are also identified (image has been modified based on the original map from www.usgs.gov).

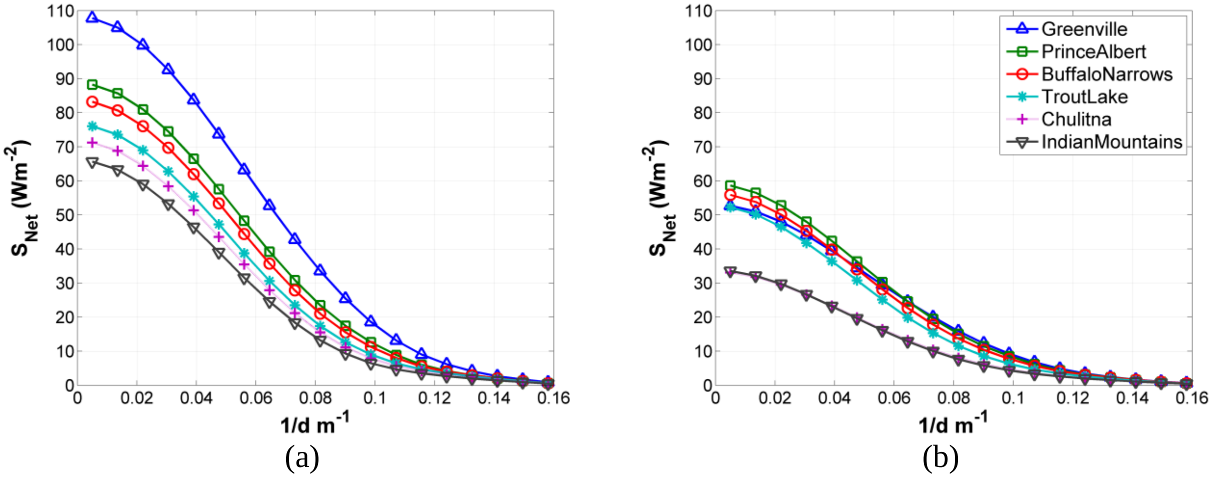

Figure 2. Variations of net shortwave radiation on level forests with vegetation density at different sites in: (a) clear and (b) interspersed cloudy sky conditions. Legend lists the sites in increasing order of latitude from top to bottom.

(a)

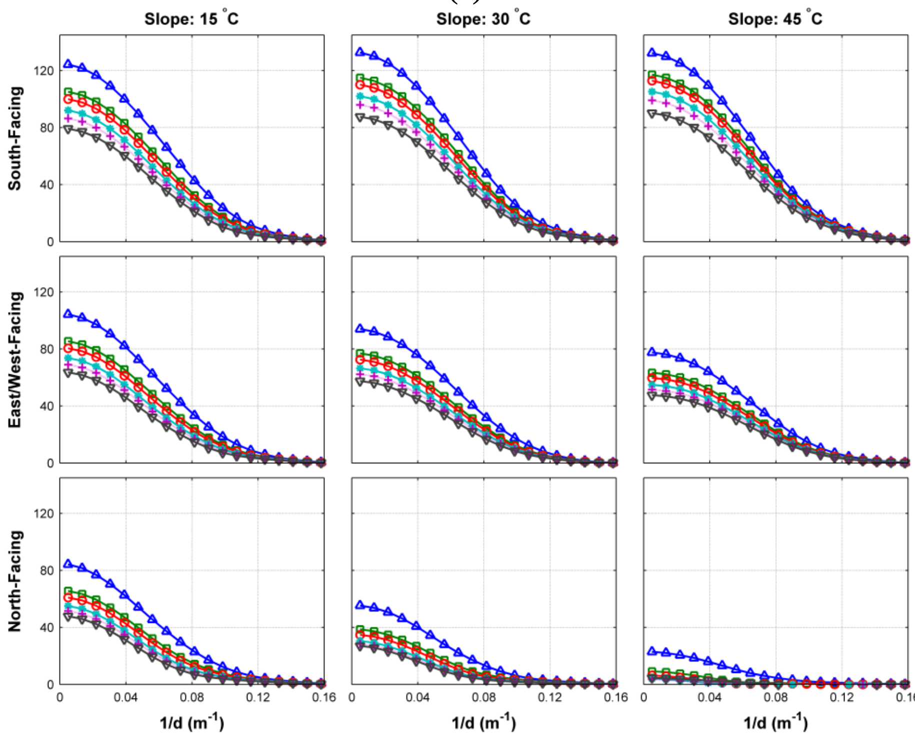

(b)

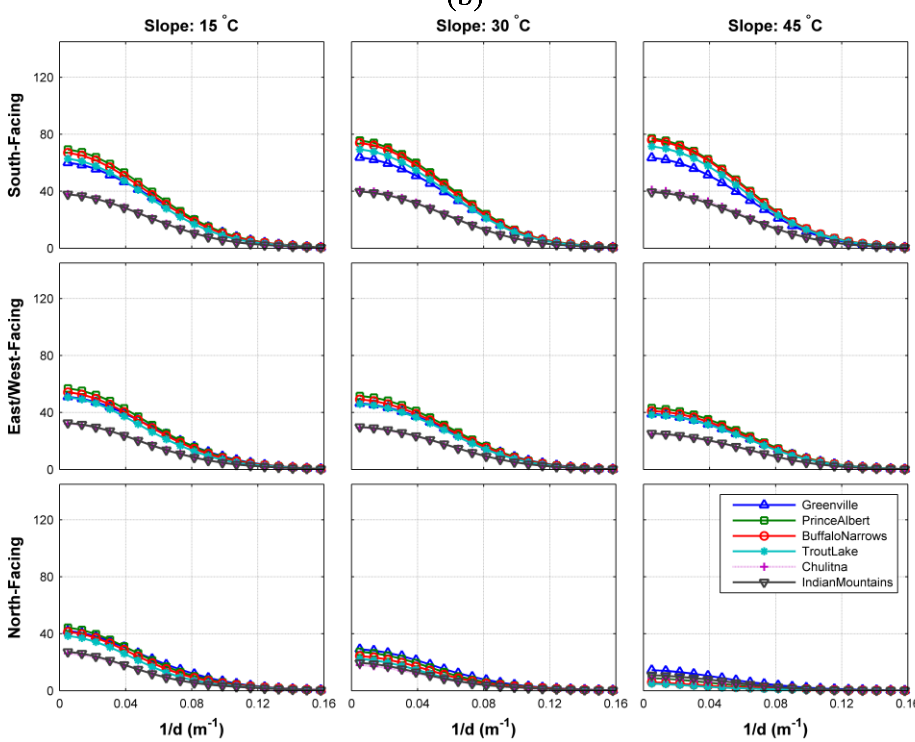

Figure 3. Variations of net shortwave radiation with vegetation density at different sites for different slope angle and aspect of the forested hillslope in: (a) clear and (b) interspersed cloudy sky conditions. Legend lists the sites in increasing order of latitude from top to bottom.

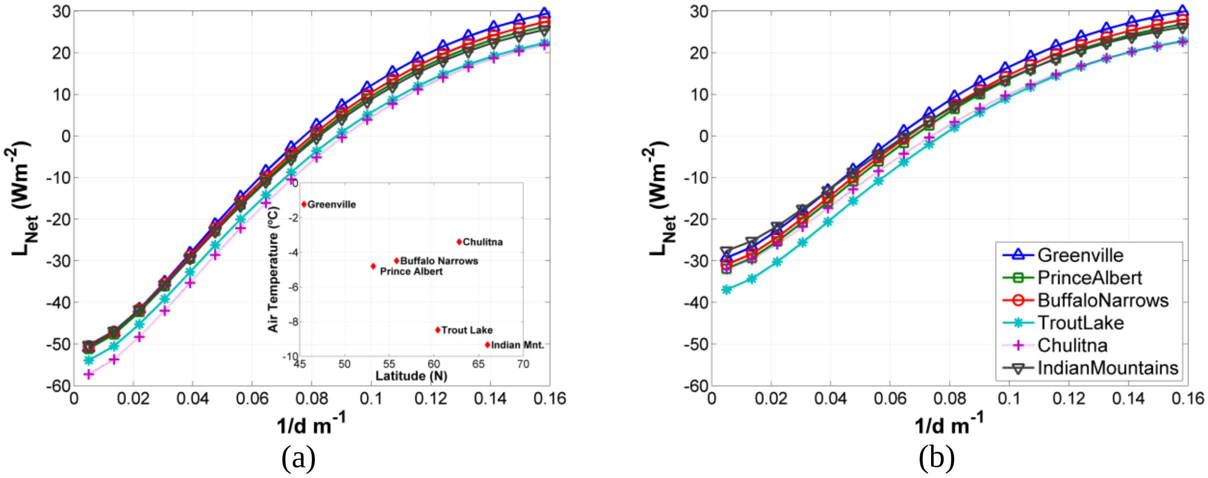

Figure 4. Variations of net longwave radiation on level forests with vegetation density at different sites in: (a) clear (inset: seasonal average air temperature), and (b) interspersed cloudy sky conditions. Legend lists the sites in increasing order of latitude from top to bottom.

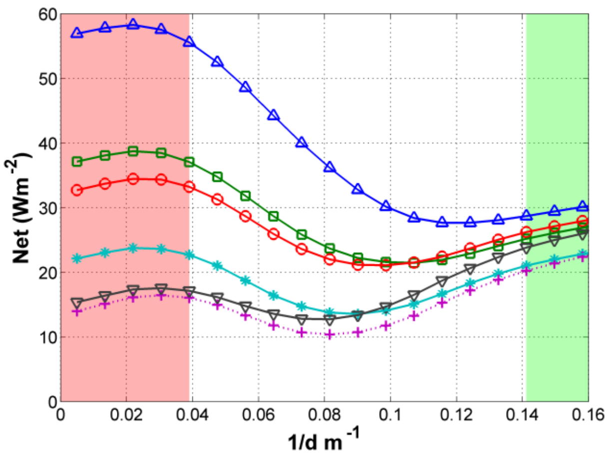

(a)

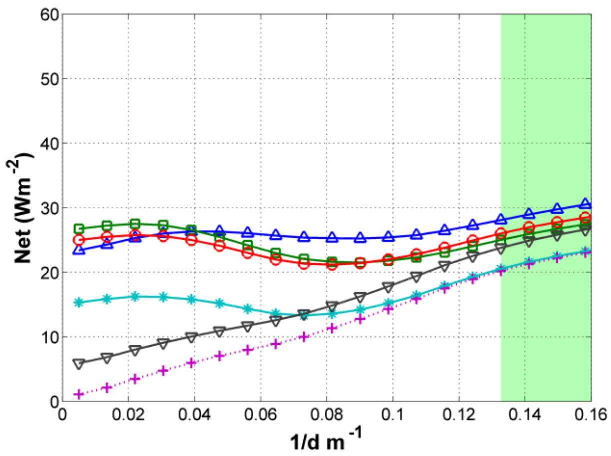

(b)

Figure 5. Variations of net radiation on level forests with vegetation density at different sites in: (a) clear and (b) interspersed cloudy sky conditions. Sites are listed in increasing order of latitude. The red and green bands indicate the vegetation densities for which shortwave ($\Delta S_{Net}/\Delta L_{Net}$>5) and longwave ($\Delta L_{Net}/\Delta S_{Net}$>5) radiation components dominantly control the variation with latitude, respectively. Δ denotes the range of respective energy component across all six sites.

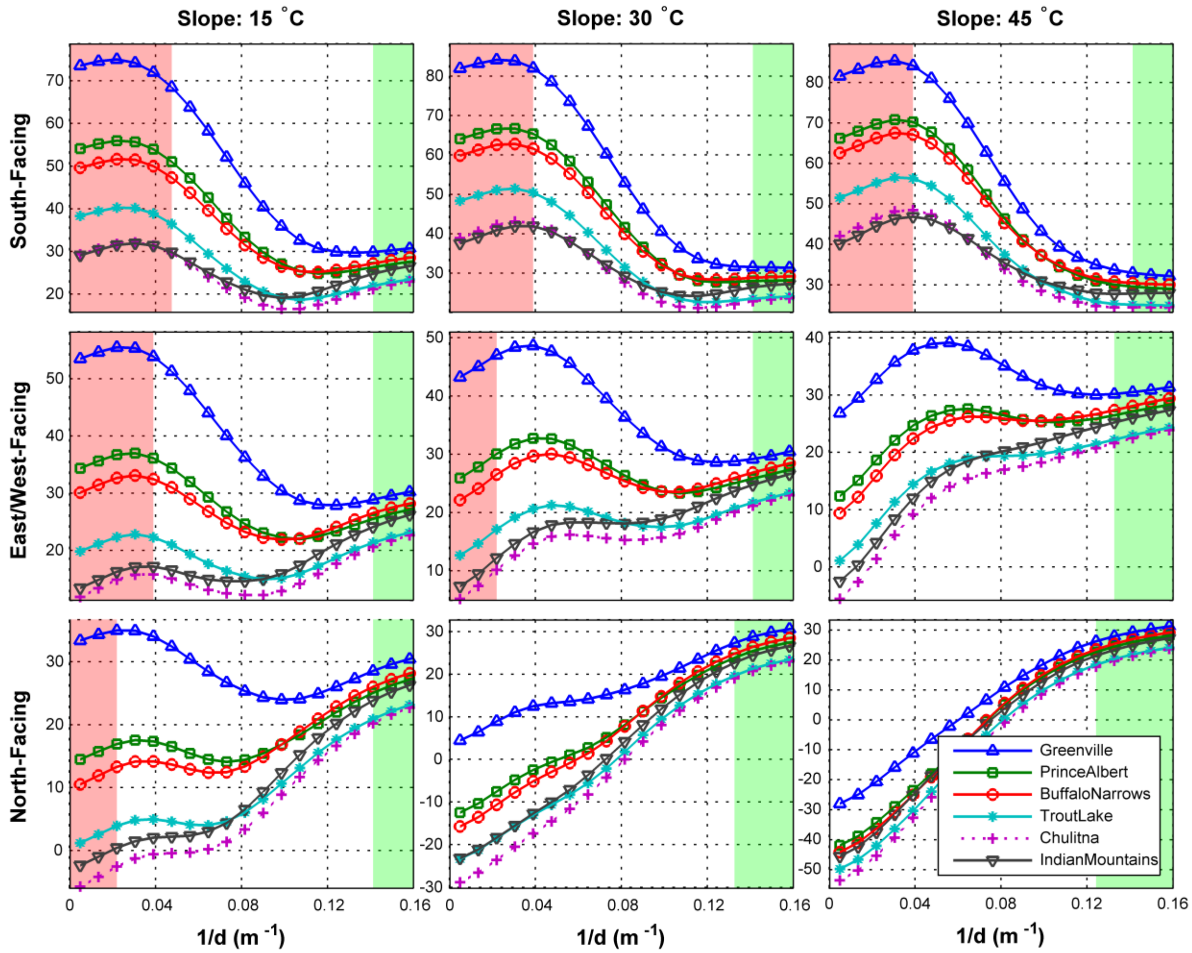

Figure 6. Variations of net radiation with vegetation density at different sites for different slope angles and aspects of the forested hillslope in clear sky conditions. Sites are listed in increasing order of latitude. The red and green bands indicate the vegetation densities for which shortwave ($\Delta S_{Net}/\Delta L_{Net}$>5) and longwave ($\Delta L_{Net}/\Delta S_{Net}$>5) radiation components dominantly control the variation with latitude, respectively. Δ denotes the range of respective energy component across all six sites.

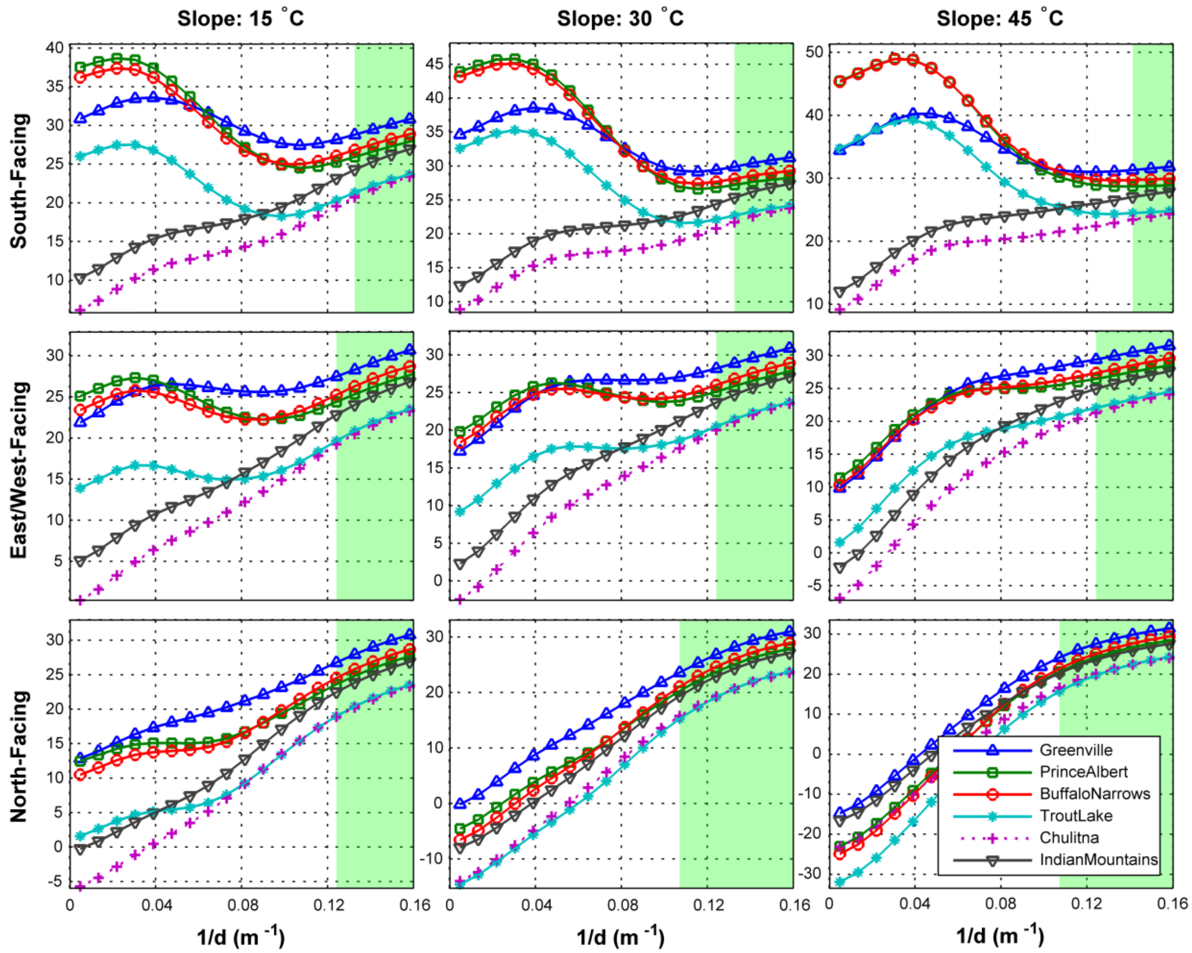

Figure 7. Variations of net radiation with vegetation density at different sites for different slope angles and aspects of the forested hillslope in interspersed cloudy sky conditions. Sites are listed in increasing order of latitude. The red and green bands indicate the vegetation densities for which shortwave ($\Delta S_{Net}/\Delta L_{Net}$>5) and longwave ($\Delta L_{Net}/\Delta S_{Net}$>5) radiation components dominantly control the variation with latitude, respectively. Δ denotes the range of respective energy component across all six sites.